

## A new multiscale modeling method for simulating the loss processes in polymer solar cell nanodevices

Anton Pershin, Sergii Donets, and Stephan A. Baeurle

Citation: *J. Chem. Phys.* **136**, 194102 (2012); doi: 10.1063/1.4712622

View online: <http://dx.doi.org/10.1063/1.4712622>

View Table of Contents: <http://jcp.aip.org/resource/1/JCPSA6/v136/i19>

Published by the [American Institute of Physics](http://www.aip.org).

---

### Additional information on *J. Chem. Phys.*

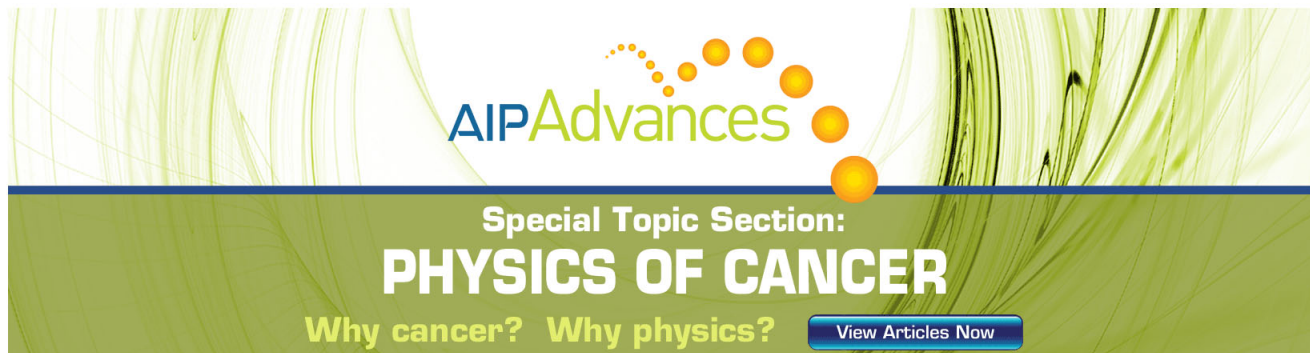
Journal Homepage: <http://jcp.aip.org/>

Journal Information: [http://jcp.aip.org/about/about\\_the\\_journal](http://jcp.aip.org/about/about_the_journal)

Top downloads: [http://jcp.aip.org/features/most\\_downloaded](http://jcp.aip.org/features/most_downloaded)

Information for Authors: <http://jcp.aip.org/authors>

## ADVERTISEMENT



AIPAdvances

Special Topic Section:  
**PHYSICS OF CANCER**

Why cancer? Why physics? [View Articles Now](#)

# A new multiscale modeling method for simulating the loss processes in polymer solar cell nanodevices

Anton Pershin, Sergii Donets, and Stephan A. Baeurle<sup>a)</sup>

*Department of Chemistry and Pharmacy, Institute of Physical and Theoretical Chemistry, University of Regensburg, D-93040 Regensburg, Germany*

(Received 21 March 2012; accepted 23 April 2012; published online 15 May 2012)

The photoelectric power conversion efficiency of polymer solar cells is till now, compared to conventional inorganic solar cells, still relatively low with maximum values ranging from 7% to 8%. This essentially relates to the existence of exciton and charge carrier loss phenomena, reducing the performance of polymer solar cells significantly. In this paper we introduce a new computer simulation technique, which permits to explore the causes of the occurrence of such phenomena at the nanoscale and to design new photovoltaic materials with optimized opto-electronic properties. Our approach consists in coupling a mesoscopic field-theoretic method with a suitable dynamic Monte Carlo algorithm, to model the elementary photovoltaic processes. Using this algorithm, we investigate the influence of structural characteristics and different device conditions on the exciton generation and charge transport efficiencies in case of a novel nanostructured polymer blend. More specifically, we find that the disjunction of continuous percolation paths leads to the creation of dead ends, resulting in charge carrier losses through charge recombination. Moreover, we observe that defects are characterized by a low exciton dissociation efficiency due to a high charge accumulation, counteracting the charge generation process. From these observations, we conclude that both the charge carrier loss and the exciton loss phenomena lead to a dramatic decrease in the internal quantum efficiency. Finally, by analyzing the photovoltaic behavior of the nanostructures under different circuit conditions, we demonstrate that charge injection significantly determines the impact of the defects on the solar cell performance. © 2012 American Institute of Physics. [<http://dx.doi.org/10.1063/1.4712622>]

## I. INTRODUCTION

Organic photovoltaic (OPV) cells have attracted increased attention in the last few years. This is essentially due to their low production costs, compared to their silicon-based inorganic counterparts.<sup>1,2</sup> The simplest OPV cell can be generated by clamping a thin layer of organic semiconducting material between two electrodes with different work functions. When the organic semiconducting phase absorbs light, electrons in the conduction band and holes in the valence band are generated. The electric field, arising from the different work functions of the electrodes, then drives the photoinduced electrons to the electrode with low work function and the holes to the opposite electrode with high work function, which induces a photocurrent. In practice, however, such solar cells possess a very small power conversion efficiency (PCE; <0.1%), since the electric field is not strong enough to separate the bound charges within the excitons. To accomplish the charge separation in an effective way, Tang<sup>3</sup> developed a two-layer OPV cell consisting of a semiconducting donor (D) material with low electron affinity and a semiconducting acceptor (A) material with high electron affinity. In such a cell, light absorption induces the creation of excitons in the material, which can diffuse in all directions through hopping processes. The fraction of excitons, reaching the DA-interfacial region also called the DA heterojunction, can be separated

into free charge carriers, where the electrons are migrating into the lowest unoccupied molecular orbital (LUMO) of the acceptor and the holes in the highest occupied molecular orbital (HOMO) of the donor. The difference in the energy levels in this case must be large enough to overcome the exciton binding energy. After the charge separation process has taken place, the electrons are transported within the A material and the holes within the D material to the respective electrodes. The migration of the charge carriers in the active layer occurs through short-ranged inter- and intra-molecular hopping processes.<sup>4</sup> In this context it should also be pointed out that the efficiency of this planar bilayer heterojunction is limited through the exciton diffusion length,<sup>5</sup> which characterizes the average distance excitons can travel through a material before annihilation occurs through geminate recombination.<sup>6</sup> In most organic semiconductors the quantity typically adopts a value of about 3–10 nm.<sup>5</sup> The excitons, which are located further apart from the DA interface than the exciton diffusion length, will have a lower probability to reach it and to be separated into free charge carriers. The active volume of this type of OPV cell is, because of the previously mentioned annihilation processes, restricted to a very small region near to the interface. However, it is generally not large enough to absorb the major part of the radiation energy and for an efficient power energy conversion. To further increase the performance of OPV cells, tremendous efforts have been realized in the last few years to develop new nanostructured materials, in which the size of the active volume is

<sup>a)</sup>Electronic mail: [stephan.baeurle@chemie.uni-regensburg.de](mailto:stephan.baeurle@chemie.uni-regensburg.de).

adjusted to accommodate the optimal exciton diffusion length. In case of the so-called bulk heterojunction (BHJ) the nanostructured morphology ensures that all excitons can reach the DA interface within the exciton diffusion length. This construction is to date the most successful OPV cell. Based on this concept, new more sophisticated device architectures have been devised in the past two decades, such as multi-layers<sup>7</sup> and blends<sup>8,9</sup> composed of different types of small molecules, bilayers<sup>10</sup> and blends<sup>11,12</sup> made from different polymer species, bilayers<sup>13</sup> and blends<sup>14–17</sup> composed of polymers and small molecules, as well as block copolymers.<sup>18</sup> However, despite recent advances, the power conversion efficiency of organic solar cells is still rather small compared to inorganic ones with maximum values ranging from 7% to 8%.<sup>19</sup>

The relatively low power conversion efficiency of OPV cells can mainly be attributed to loss phenomena of the elementary particles involved in the photovoltaic process, such as photon loss, exciton loss, and charge carrier loss.<sup>20</sup> These loss phenomena can occur during the following steps of the photovoltaic process:<sup>21</sup> (1) photon absorption and exciton generation; (2) exciton diffusion to the DA heterojunction; (3) exciton separation and charge carrier generation at the DA heterojunction; (4) diffusion of the charge carriers to the respective electrodes; and (5) collection of the charge carriers at the electrodes. With the exception of the process of exciton diffusion to the DA heterojunction, none of the previously described processes have been optimized in a satisfactory way in case of the polymer solar cell materials currently available.<sup>22</sup> Therefore, it is not surprising that their power conversion efficiency is still relatively low, compared to their inorganic counterpart. For a simultaneous optimization of the steps (1), (2), and (4), the generation of a clearly defined morphology with optimized phase thickness is of crucial importance, since it guarantees that the electrons and holes can be separated and transported to the electrodes without losses.<sup>23</sup> To achieve these goals, it is worth considering that on the one hand an active phase two times the size of the exciton diffusion length allows an efficient exciton yield, but on the other hand a too thin active phase leads to a dramatic loss of efficiency because the number of absorbed photons depends on the thickness of the absorbing material.<sup>18</sup> A further problem is to ensure that the charge carriers can be transported from the DA heterojunction to the electrodes. To optimize all steps of the photovoltaic process, one has, thus, to find an ideal compromise for the morphology as a function of the composition of the material. Therefore, the manufacturing of stable nanostructured BHJ's with continuous percolation paths for the charge carriers and phases that possess twice the size of the exciton diffusion length is a major prerequisite for the increase of the performance of polymer solar cells. However, such device architectures on the nanoscale are not easy to generate with simple DA mixtures. Although the techniques for the generation of such BHJ's can in general also be applied to this small length scale,<sup>24</sup> the thin-film structures do not remain stable over long times without the use of special compatibilisers<sup>25</sup> or crosslinking procedures,<sup>26</sup> rising their production costs significantly. Moreover, even if the blending of D- and A-phases at the nanoscale usually leads to a drastic increase of the exci-

ton dissociation efficiency, the strongly wounded morphologies generally possess numerous persistent bottlenecks and dead ends, which restrain or even prevent the diffusion of the free charge carriers to the electrodes.<sup>27</sup> As a result, these defect structures can lead to the loss of free charge carriers through charge recombination. In the same way excitons can be trapped in such structures and may relax radiatively or radiationless within picoseconds up to nanoseconds back to the ground state, leading to the loss of the excitons.<sup>22</sup> To generate tailor-made BHJ's at the nanoscale, block copolymers can be used, which due to the incompatibility of different monomer types accomplish a process of phase separation and form stable continuous DA nanostructures.<sup>28–33</sup> Several attempts to covalently link D- and A-properties in block copolymers have successfully been carried out, such as in case of DA-diblock copolymers,<sup>18,34</sup> conjugated DAD-triblock copolymers,<sup>35</sup> block copolymers based on covalent linking of conjugated and non-conjugated blocks,<sup>22</sup> as well as conjugated polymers connected to fullerene derivatives.<sup>25,36</sup> The performance of block-copolymer materials in photovoltaic cells has recently been compared with polymer-blend systems and was found to be one order of magnitude more efficient in case of block-copolymer devices of the same thickness and composition.<sup>18</sup> This great improvement was attributed to the larger active space in the interfacial region of the DA heterojunction, which results from interfacial mixing of the D- and A-segments. A further till now only sparsely explored issue is the influence of the local structural characteristics, such as defects and impurities, on the previously mentioned loss processes and their consequence on the performance of polymer solar cells. Recent experiments indicate that such structural characteristics can strongly affect the complementary processes of charge generation and charge recombination as well as the process of charge transport to the electrodes. For example, Coffey and Ginger<sup>37,38</sup> observed very recently with time-resolved electrostatic force microscopy that, contrary to the common belief,<sup>39</sup> the domain centers of their DA-polyfluorene blends provide a much greater contribution to the photocurrent than the region in close proximity to the DA heterojunctions. They explained their observations by the mixing of the D- or A-rich phases with a minority fraction of the other component, which affects charge generation as well as charge transport. In a further experimental investigation McNeill *et al.*<sup>40</sup> found by applying scanning transmission x-ray microscopy to similar polyfluorene blends that the interfacial regions, enriched with the A component, may provide preferential pathways for electron transport. Moreover, in a recent work Wang *et al.*<sup>41</sup> speculated that the charge transport can severely be affected by intra-molecular defects, such as kink defects and chemical impurities. Finally, it is also well-known from several experimental and theoretical studies<sup>4,27,37,38,40,42</sup> that small changes in the production or processing conditions can have large effects on the number and shape of structural inhomogeneities, leading to strong variations in the performance of the resulting devices. In conclusion, the previous discussion indicates that the local structural characteristics of polymer solar cell materials exhibit a major influence on the processes of exciton and charge carrier loss. Therefore, detailed theoretical

and experimental investigations are required to understand their consequences on the device performance and to devise new strategies to engineer polymer solar cells with optimized opto-electronic properties.

The goal of our paper is to study the relationship between the local structural characteristics and the processes of charge carrier and exciton loss in nanostructured polymer solar cells, and to make use of the gained knowledge for exploring new routes to optimize their photovoltaic behavior. To this end, we introduce a new computer simulation approach by coupling a mesoscopic field-theoretic method with a suitable dynamic Monte Carlo (DMC) algorithm, which allows to simulate the elementary photovoltaic processes involving the charge carriers and excitons within a particle description. Using this algorithm, we investigate the impact of the morphological characteristics of a novel phase-separated nanostructured DA-polymer blend at different degree of phase separation and under various charge-injection conditions on its photovoltaic properties.

Our paper is organized in the following way. In Sec. II we provide a short review about existing simulation methods to model solar cell devices, followed by the introduction of the new simulation approach used in this work. Afterwards, in Sec. III we present simulation results from its application on a DA-polymer blend and discuss them with regard to data from recent experiments. Finally, we end our paper with a summary and a brief outlook.

## II. METHODS AND SIMULATION DETAILS

Most of the computer simulation methods for investigating the photovoltaic behavior of solar cell devices make use of the drift-diffusion model.<sup>42</sup> It bases on a continuum treatment of the system and enables the description of the diffusion of charge carriers in the electric field along concentration gradients. The dynamic evolution of the model is obtained through the self-consistent solution of the continuity equations for the electrons and holes as well as Poisson's equation. It has so far successfully been employed to investigate the photovoltaic behavior of inorganic semiconducting devices and has recently also been adapted to organic devices. However, till now most of the modeling works relying on the drift-diffusion model have essentially dealt with the simulation of organic light emitting diodes.<sup>42</sup> By contrast, only little attention has been put on the exploration of photovoltaic devices. In the year 2003, Gregg and Hanna<sup>43</sup> first demonstrated on a simple pedagogical example the fundamental difference between inorganic and OPV-cell devices. To this end, they adapted the conventional one-dimensional drift-diffusion model of inorganic systems to the case of organic systems, where electrons and holes can only be generated at the DA interfaces. This technique enables the description of the diffusion of the charge carriers in polymer solar cells along the internal concentration gradients. However, it does not permit to take into account the generation, diffusion, and dissociation of the excitons. Barker *et al.*<sup>44</sup> improved the drift-diffusion model for organic devices by explicitly incorporating the fraction of light, leading to charge separation at the interfaces, and could achieve in this way a good agreement with the experimental

results. However, also in this model the exciton behavior was only included in an indirect way. In a further work Härter *et al.*<sup>45</sup> considered a prototypical one-dimensional device with a broader DA-interfacial region, to study the consequences of blending on the solar cell performance. In the model they restricted the generation of electrons and holes to the interfacial region and allowed the charge carriers to migrate through the entire system by taking into account the existence of the interfaces. However, the effect of the morphology was here only included through a simple unidirectional change of the properties. Recently, Buxton and Clarke<sup>27,42</sup> developed a new simulation procedure on the basis of a two-dimensional drift-diffusion model to investigate the influence of the morphology on the photovoltaic behavior of phase-separated block-copolymer solar cells. In this technique the morphology of a diblock-copolymer system is determined *a priori* with the mesoscopic Flory-Huggins-Cahn-Hilliard method, which relies on the mean-field (MF) approximation. The structural information is then used as input for the self-consistent solution of the continuity-transport equations for the electrons, holes, and excitons in conjunction with Poisson's equation. However, the general applicability of this method, despite its low computational expense, remains rather limited. On the one hand the MF approximation neglects the concentration fluctuations of the monomers and, therefore, only provides reliable informations in the range of soft monomer interactions about the system. On the other hand the drift-diffusion model does not allow the explicit description of local particle processes, e.g., the loss processes of charge carriers through interaction with other charge carriers at bottlenecks and dead ends of the morphology. In the underlying continuum description of the system, local particle phenomena are only taken into account in an implicit way through the macroscopic parameters of the model. A correct representation and investigation of these phenomena require in contrast an atomistic or even better a quantum-mechanical description of the system. However, these levels of description are computationally very demanding and, thus, have only rarely been employed up to now.<sup>46</sup> Moreover, phenomena occurring in complex polymer materials are typical multiscale problems.<sup>47</sup> A suitable multiscale modeling tool therefore should be able to treat several processes at different levels of description simultaneously within one single simulation. In case of OPV applications the important length scales range from the quantum-mechanical level, such as the description of absorption processes of photons in nanophase-separated block-copolymer matrices, up to the mesoscopic level of description, in which millions of atoms of the polymer matrix determine the nanostructure and, thus, the performance of the device. The latter length scale strongly influences both the transport properties, such as the conductivity of the free charge carriers,<sup>27,42</sup> as well as the macroscopic properties, such as the linear mechanical properties,<sup>48</sup> of the entire device. Due to the diversity and complexity of the nanodevice applications, only a few generally applicable multiscale modeling methods have been devised up to now, which allow to treat OPV applications in a reliable way. A few promising methods in the traditional particle description have recently been used for the modeling

of polymers on metal surfaces.<sup>49–51</sup> However, we can safely predict that numerous polymer solar cell devices will only hardly be treatable within the conventional particle description, due to the large system sizes and long chain lengths encountered in most polymer applications.<sup>47</sup>

To study the influence of defects on the solar cell performance, we developed a new simulation algorithm, which makes use of both either the time-dependent Ginzburg-Landau (TDGL) method or the self-consistent field theory (SCFT) method,<sup>52</sup> to generate the nanoscale morphology of the polymer blend, in conjunction with the dynamic Monte Carlo method, to mimic the elementary photovoltaic processes. To obtain morphologies of different interfacial lengths, we describe the non-equilibrium dynamics of the phase-separation process using the TDGL method. The method is based on the Cahn-Hilliard-Cook (CHC) nonlinear diffusion equation for a binary mixture, which for an incompressible binary AB-polymer blend results in the following equation of motion:<sup>52,53</sup>

$$\frac{\partial \phi(\mathbf{r}, t)}{\partial t} = \nabla \cdot \left\{ M \nabla \frac{\delta F[\phi(\mathbf{r}, t)]}{\delta \phi(\mathbf{r}, t)} \right\} + \eta(\mathbf{r}, t). \quad (1)$$

Here,  $\phi(\mathbf{r}, t)$  represents the local spatiotemporal monomer concentration for species A and  $M$  is the mobility, whereas  $\eta(\mathbf{r}, t)$  is a thermal noise term with zero mean and a variance given by the fluctuation-dissipation theorem, i.e.,  $\langle \eta(\mathbf{r}, t) \eta(\mathbf{r}', t') \rangle = -2Mk_B T \nabla^2 \delta(\mathbf{r} - \mathbf{r}') \delta(t - t')$ . In the latter expression  $\delta(\mathbf{r} - \mathbf{r}')$  defines a delta function, while  $T$  and  $k_B$  are the temperature and Boltzmann's constant, respectively. For the free energy of the polymer blend, we make use of the following functional:<sup>52</sup>

$$\frac{F[\phi(\mathbf{r}, t)]}{k_B T} = \int d\mathbf{r} \left[ \frac{f_{FH}[\phi(\mathbf{r}, t)]}{k_B T} + \kappa(\phi) |\nabla \phi(\mathbf{r}, t)|^2 \right], \quad (2)$$

where

$$\frac{f_{FH}[\phi(\mathbf{r}, t)]}{k_B T} = \frac{\phi(\mathbf{r}, t)}{N_A} \ln \phi(\mathbf{r}, t) + \frac{1 - \phi(\mathbf{r}, t)}{N_B} \ln [1 - \phi(\mathbf{r}, t)] + \chi \phi(\mathbf{r}, t) [1 - \phi(\mathbf{r}, t)] \quad (3)$$

is the Flory-Huggins (FH) free energy of mixing with  $\chi$  as the enthalpic interaction parameter, while  $N_A$  and  $N_B$  represent the degrees of polymerization of the components A and B, respectively. We point out that the second term in Eq. (2) energetically penalizes the occurrence of concentration gradients and induces the coarsening of the domains.<sup>27</sup> The coefficient  $\kappa$  for an incompressible polymeric system can be expressed as

$$\kappa(\phi) = \frac{1}{36} \left[ \frac{l_A^2}{\phi(\mathbf{r}, t)} + \frac{l_B^2}{[1 - \phi(\mathbf{r}, t)]} \right], \quad (4)$$

where  $l_i$  is the Kuhn length of species  $i$ . To solve the previous system of equations, we have discretized the CHC equation in Eq. (1) and solved it numerically, using the finite-difference technique<sup>54</sup> with a mobility parameter of  $M = 10$ . In our calculations we considered a system with a discrete lattice of size  $32 \times 32$ , composed of a symmetric AB-homopolymer blend with  $N_A = N_B = 10$  and  $l_A = l_B = l$ , as well as an enthalpic interaction parameter  $\chi = 0.5$ . For the numerical integration, we used a time step of 0.01 with a maximum number of simulation steps of 5000. To

obtain the equilibrium configuration that would be extracted from the phase-separation process of the AB-polymer blend at infinite times, we make use of the static SCFT method, which provides the distribution of segment volume fractions at equilibrium. For a detailed derivation of the SCFT method and description of its implementation, we refer to Refs. 55 and 56, respectively. To compute the morphologies, we made use of the program package OCTA (Refs. 54 and 57) and performed the solar cell simulations with our DMC algorithm for each of the morphologies, as described in the following.

To simulate the overall photovoltaic process, we consider in our algorithm that three types of mobile particles, i.e., electrons, holes, and excitons, are present in the polymer solar cell device. Depending on their local structural environment and situation, several events are available for these particles, which are summarized in the following:

1. exciton generation by light absorption;
2. exciton motion within the material through diffusion or exciton annihilation through geminate recombination;
3. exciton dissociation at the heterojunction with creation of an electron and a hole;
4. charge recombination or charge motion under the influence of the built-in field from the difference between the electrode work functions;
5. charge collection at the appropriate electrodes.

To demonstrate the predictive power of our simulation approach, we consider a novel DA-polymer blend composed of poly(perylenediimide-alt-dithienothiophene) (PPDI-DTT) and bis(thienylenevinylene)-substituted polythiophene (biTV-PT). In Fig. 1 we plot the corresponding chemical structures of the DA-polymer blend components. In the calculations we use a system's temperature of  $T = 298$  K and a lattice size of  $32 \times 32$  sites with a lattice constant of  $a_0 = 1$  nm as well as periodic boundary conditions applied in all directions. At each lattice site, we impose a single occupancy constrain for the charge carriers as well as the excitons. Moreover, we suppose that the majority component at each lattice site determines whether the site is either part of the electron-conducting or hole-conducting phase, which is a reasonable approximation in case of highly phase-separated polymer-blend morphologies, where the regions of segmental mixing at the interfaces are small. We further assume that the particle motion within the system occurs through hopping between different lattice sites. These hopping processes together with the other available processes constitute the queue of events, which determines the sequence of configurational changes that can take place during the system's evolution through phase space. Each possible event is associated with a waiting time given by

$$\tau_\omega = -\frac{1}{\omega} \ln(\xi), \quad (5)$$

where  $\omega$  is the rate of an event, while  $\xi$  is a randomly distributed number between 0 and 1. To accomplish the dynamical evolution, we use the first reaction method (FRM),<sup>58,59</sup> which implies that all possible events are stored in a queue in order of ascending waiting times. At each simulation step, the event with the smallest waiting time at the onset of the queue

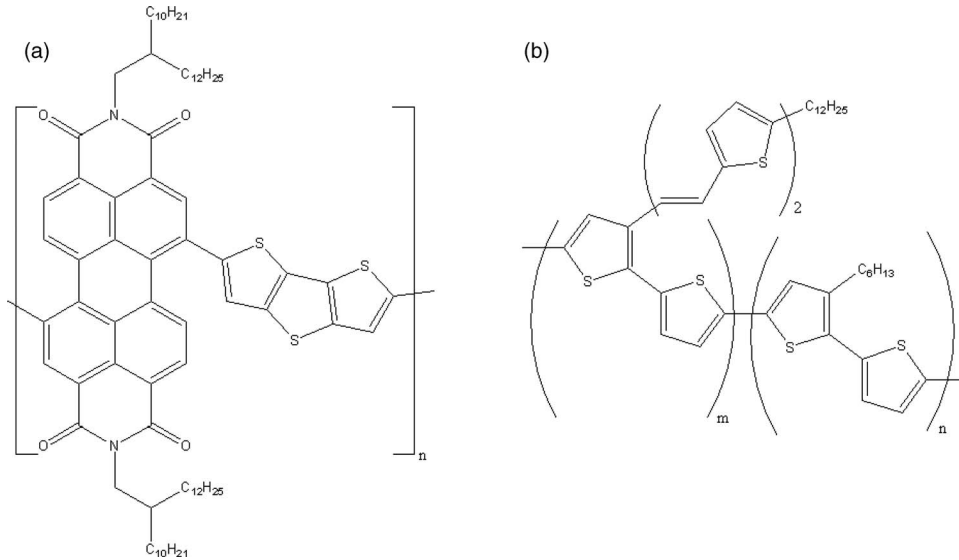


FIG. 1. Chemical structure of the DA-polymer blend PPDI-DTT-biTV-PT composed of (a) poly(perylene diimide-alt-dithienothiophene) and (b) bis(thienylenevinylene)-substituted poly-thiophene.<sup>59</sup>

is chosen and carried out. Finally, this event is removed from the queue and the simulation time is incremented by the respective waiting time. We should point out in this regard that the queue of events needs to be permanently updated to sample the full configuration space of the system. This implies that the execution of a specific event can cause the change in a chain of related subsequent events and, thus, requires the renewal of the queue accordingly. The excitons are created at randomly chosen sites in the lattice with a constant rate  $\omega_{cre} = 900 \text{ s}^{-1} \text{ nm}^{-2}$ , which is calculated from the AM1.5 solar spectrum with illumination of  $90 \text{ mW/cm}^2$  and the absorption spectrum of the polymer blend.<sup>59,60</sup> The exciton hopping rate from the lattice site  $i$  to a nearby site  $j$  is given by<sup>59</sup>

$$\omega_{ij} = \omega_e \left( \frac{r_0}{r_{ij}} \right)^6, \quad (6)$$

where  $r_{ij}$  denotes the distance between the hopping sites  $i$  and  $j$ , while  $r_0 = 10 \text{ nm}$  is the exciton-localization radius and  $\omega_e$  is the hopping-attempt frequency. The excitons on the lattice are allowed to jump within a radius of  $15 \text{ nm}$  in either the hole- or electron-conducting phase. The prefactor  $\omega_e r_0^6 = 2 \text{ nm}^6 \text{ ps}^{-1}$  and exciton recombination rate  $\omega_{dec} = 0.002 \text{ ps}^{-1}$  are selected, to reproduce the experimental values of exciton diffusion length ( $\sim 10 \text{ nm}$ ) and lifetime ( $\sim 500 \text{ ps}$ ). The hopping rate of charge carriers is calculated using the formula of the Marcus theory<sup>46,61</sup>

$$\omega_{ij} = V_{hop} \exp \left[ -\frac{(E_i - E_j + \lambda)^2}{4\lambda k_B T} \right], \quad (7)$$

where  $E_i$  and  $E_j$  designate, respectively, the energies of hopping sites  $i$  and  $j$ , while  $\lambda$  is the reorganization energy corresponding to twice the polaronic binding energy.<sup>62</sup> The prefactor,  $V_{hop}$ , is derived from the Einstein relationship under isoenergetic site condition<sup>4,46</sup> and is given by

$$V_{hop} = \frac{6k_B T \mu_{e/h}}{qa_0^2} \exp \left[ \frac{\lambda}{4k_B T} \right], \quad (8)$$

where  $\mu_{e/h}$  is the mobility of the electrons/holes with charge  $q$  in both polymer species and is taken as  $\mu_{e/h} = 10^{-3} \text{ cm}^2 \text{ V}^{-1} \text{ s}^{-1}$ . Note that in our simulations we assumed the electrons and holes to have equal mobility and, thus, we chose for both charge carrier types  $V_{hop} = 1.06 \times 10^{-2} \text{ ps}^{-1}$ . The energy of the electron, created either by migration or by injection, at the hopping site  $i$  is defined as<sup>63</sup>

$$E_i = \phi_w + \Delta_{inj} - eFx_i - \frac{e^2}{16\pi\epsilon_0\epsilon_r x_i}, \quad (9)$$

where  $\phi_w$  represents the work function of the Al contact at the electrode,  $\Delta_{inj}$  is the injection barrier,  $F$  is the net field resultant from the built-in voltage and applied bias,  $x_i$  is the distance from the contact, and  $e$  is the electron charge magnitude. The final term in Eq. (9) describes the contribution of the polarization of the electrodes (image charge effect) for a material of dielectric constant  $\epsilon_0\epsilon_r$ , where  $\epsilon_0$  is the vacuum permittivity and  $\epsilon_r = 3.5$  the relative permittivity. Note that an equivalent expression has been used for the hole transport. Moreover, to take into account the Coulombic interaction of the charge at site  $i$  with all other charges within the system, we further add to the energy difference  $E_i - E_j$  in Eq. (7) the following contribution:<sup>63</sup>

$$\Delta E = \sum_{j=1}^n \frac{qe}{4\pi\epsilon_0\epsilon_r r_{ij}}, \quad (10)$$

where  $n$  is the total number of other charges in the system with  $q = +e$  for electron-electron and hole-hole repulsion as well as  $q = -e$  for electron-hole attraction. To treat the long-range tail of the electrostatic contribution, we have cut the Coulomb potential at  $r_c = 10 \text{ nm}$  and shifted the function to zero. In addition, we assumed that, if an electron and hole are located on adjacent sites, they can recombine with the rate  $\omega_{rec} = 10^{-6} \text{ ps}^{-1}$ . Finally, we considered the system to be equilibrated when the deviations in the values of exciton dissociation efficiency, charge transport efficiency, and

exciton lifetime did not exceed the preset error of 0.01% within a certain timespan at the end of the simulation.

To study the influence of the charge injections at the electrodes on the device performance, we have taken into account three different circuit conditions. An open circuit represents the case without charge injection at the system's boundaries, where no current flows externally due to the infinite resistance in the circuit.<sup>59</sup> To realize a short circuit, we impose that any collected charge leaving the system's boundary at one electrode passes through the external circuit with zero resistance and is re-injected at the opposite electrode by fulfilling the condition of electroneutrality for the overall system. In case of a real circuit we consider a closed circuit, where the charge injections at the electrodes take place via hopping of the charges from the Fermi level of the electrode material over the charge-injection barrier to an adjacent polymer site in the first monolayer.<sup>59</sup> At each electrode site, i.e., at a junction between electron conductor and cathode or hole conductor and anode, a charge carrier can be injected at a time interval determined by its characteristic injection rate. The injection rate is calculated using the Marcus formula in Eq. (7) by considering that the difference in the energies  $E_i - E_j$  equals the energy barrier between the LUMO of polymer type 1 and the Fermi level of Al, i.e., the energy barrier for charge injection  $E_{IB} = 0.4$  eV.<sup>59</sup> The injection process is then included into the queue of events of the FRM algorithm.

### III. RESULTS AND DISCUSSION

We start the analysis of our simulation results by considering the structural characteristics of our system, composed of the AB-polymer blend PPDI-DTT-biTV-PT introduced previously. In Fig. 2 we show the corresponding morphologies, obtained either with the CHC-TDGL (A-H) or the CHC-SCFT method (I) [red: A phase (electron conducting); blue: D phase (hole conducting)].

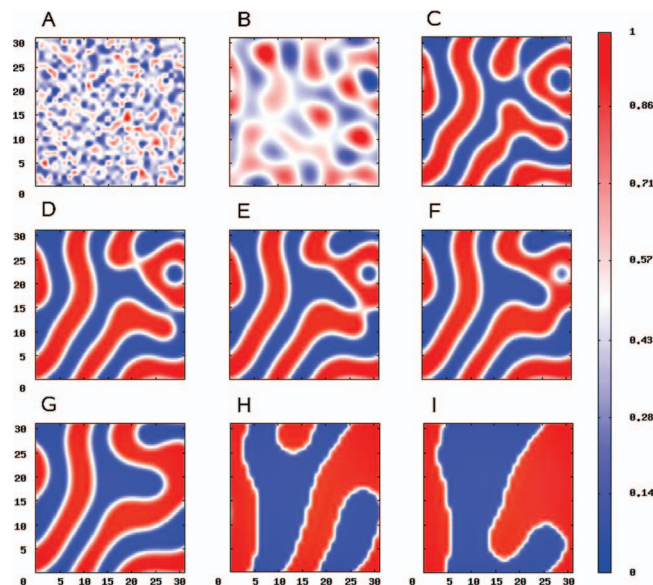


FIG. 2. Morphologies of the DA-polymer blend PPDI-DTT-biTV-PT at different scale of phase separation as a function of the volume fractions of the monomer types obtained either with the CHC-TDGL (A-H) or the CHC-SCFT method (I) [red: A phase (electron conducting); blue: D phase (hole conducting)].

method (I), at different scale of phase separation as a function of the volume fractions of the monomer types. We observe that with increasing simulation time the morphology acquires an increasing degree of phase separation with decreasing interfacial length and changes successively from unordered to lamellar-like structure. Moreover, we see that a point defect structure is created in the upper right corner of the 2D diagram, starting from morphology B up to morphology F. In case of the morphologies C and D we observe that the defect structure transforms into an isolated inclusion, where the A and D phases are completely disconnected from the rest of the phases resulting in the creation of several dead ends. Then, at the transition from morphology E to F the A phase at the inclusion becomes continuous, whereas the D phase becomes fully continuous only at the transition from morphologies F to G. Next, in Fig. 3 we show the corresponding results for the charge transport efficiency, exciton dissociation efficiency, and internal quantum efficiency (IQE) for the phase-separated DA-polymer blend PPDI-DTT-biTV-PT as a function of interfacial length under open-circuit, short-circuit, as well as real-circuit conditions. From Fig. 3(a), we deduce that with increasing interfacial length the exciton dissociation efficiency, representing the ratio of the number of dissociated excitons to the number of generated excitons, increases steadily in the range from 60 to 95 nm, corresponding to the morphologies from I to G. In the range of morphologies from F to A, the quantity undergoes a change in slope, which relates to the fact that in this regime the nanophases become thinner and the DA-polymer blend adopts increasingly more discontinuous structural characteristics. The thinning of the phases reduces the average distance excitons have to travel before they can dissociate into charge carriers at the interfaces and, thus, ensures a higher exciton dissociation efficiency. By contrast, we deduce from Fig. 3(b) that the charge transport efficiency, reflecting the ratio of the number of charge carriers exciting the device versus twice the number of the dissociated excitons, decreases with increasing interfacial length for all three charge-injection cases. After a slow steady decrease starting from 100% efficiency in the range from 60 up to 95 nm (I-G), the curves undertake a sharp drop in efficiency of about 60% at an interfacial length of 100 nm under real-circuit and open-circuit conditions, which corresponds to the range of morphologies from G to D. Moreover, it is apparent that the largest losses in efficiency take place at the transition between the morphologies E and D. By contrast, in the short-circuit case the charge transport efficiency at the same interfacial length undergoes only a smooth stepwise decrease of about 20%. In all three cases the regimes of major efficiency loss are followed by a range of slow steady decrease with diminishing degree of phase separation of the DA-polymer blend up to the disordered morphology A. However, we note that in this regime the charge transport efficiency in the short-circuit case remains at much higher level, compared to the real-circuit and open-circuit case. Next, we compare these results with the ones for the internal quantum efficiency in Fig. 3(c), which designates the ratio of the number of charge carriers collected at the electrodes versus twice the number of generated excitons. We observe that the quantity for all three charge-injection conditions exhibits a maximum with

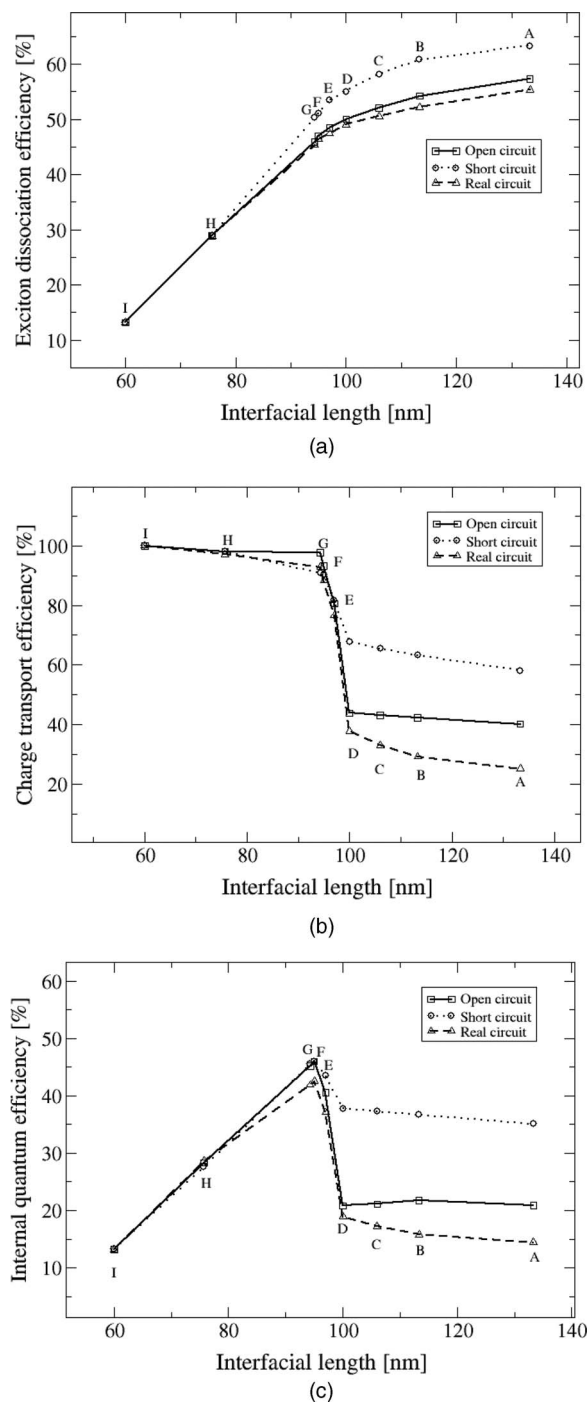


FIG. 3. Exciton dissociation efficiency (a), charge transport efficiency (b), and internal quantum efficiency (c) of the phase-separated DA-polymer blend PPDI-DTT-biTV-PT as a function of interfacial length under open-circuit, short-circuit, as well as real-circuit conditions, obtained either with the DMC-CHC-TDGL (A-H) or the DMC-CHC-SCFT method (I).

a peak at an interfacial length of 95 nm, which corresponds to the morphology F. With decreasing degree of phase separation the quantity experiences a sharp drop of about 25% under open-circuit and real-circuit conditions, whereas in the short-circuit case the drop in efficiency amounts only to 10%. The sharpest decline in the IQE in all cases takes place in the range of interfacial lengths between 97 nm and 100 nm, which corresponds to the range of morphologies between F

and D. By comparing these results to the ones of the charge transport and exciton dissociation efficiency in Figs. 3(a) and 3(b), we conclude that at low interfacial lengths the IQE is primarily restricted by a low exciton dissociation efficiency, whereas at high interfacial lengths the IQE is essentially limited by a low charge transport efficiency. At the maximum IQE, the best compromise between the efficiencies of exciton dissociation and charge transport is found, which results in the maximum device performance. Moreover, we find that the charge-injection conditions determine in a decisive way the magnitude of the quantity, which shows that they need to be taken into account adequately in the computer simulation of loss process of polymer solar cell devices.

To study in more detail the causes for this dramatic change in the charge transport and internal quantum efficiencies with the scale of phase separation of the polymer blend, we analyze in Fig. 4 the corresponding distribution of the charge carriers under real-circuit conditions for the morphologies presented previously. In case of the disordered morphology A, we see that the charges are captured and accumulated within the numerous traps of the weakly phase-separated nanostructure. Due to the small phase thickness, only a few excitons are lost on the route to the DA interface. Thus, most of them become separated into charge carriers, which may accumulate and then recombine restricting their lifetime in the confined region of space. A major performance-limiting factor of such morphologies is that their charge transport to the electrodes is dramatically impaired because of the lack of continuous percolation paths to the electrodes. In case of the morphologies B to D with moderate degree of phase separation, we observe that the charge carriers are captured and accumulated in several dead ends and bottlenecks, severely reducing their efficiency of charge transport to the electrodes. In particular, we see that at the point defects and at the dead

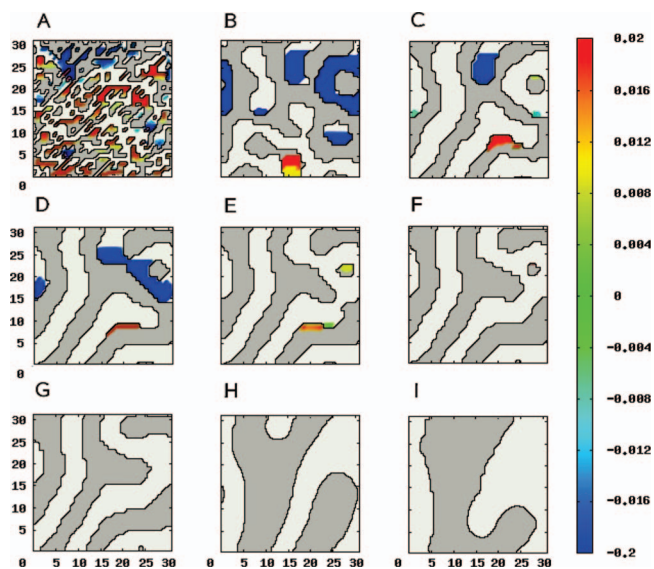


FIG. 4. Charge density of the phase-separated DA-polymer blend PPDI-DTT-biTV-PT for morphologies with different scale of phase separation under real-circuit conditions, obtained either with the DMC-CHC-TDGL (A-H) or the DMC-CHC-SCFT method (I) [light grey: A phase (electron conducting); dark grey: D phase (hole conducting)]. Electrodes are applied in horizontal direction for all morphologies.



ends in the upper left and right corner of the 2D diagram a significant amount of electrons is accumulated. This relates to the fact that the charges under the action of the electrical field, resulting from the difference in electrode work functions, are trapped in these defect structures and can only decay through charge recombination at the DA interfaces. Similarly, the holes are strongly concentrated in a notch, formed by the D phase, and remain trapped in this region, due to the influence of the external electrical field from the electrodes as well as the internal fields from the nearby accumulated electrons. Moreover, we deduce from morphology C that isolated inclusions, which are fully disconnected from the electrodes are not able to function as effective charge traps. In conclusion, we see that the charge transport is severely hindered and, thus, the IQE is severely reduced in cases where the A and D phases are partially discontinuous, but remain connected to the electrodes to some extent. This demonstrates the important influence of the charge injection at the electrodes on the charge accumulation at the defect structures and the overall charge transport efficiency, as confirmed by Fig. 3(b). It is also worth noting in this regard that the high charge transport efficiency for the short-circuit case, in contrast to the real-circuit and open-circuit case, for morphologies A to D correlates with the reduced accumulation of the free charge carriers in the defect structures, as we can deduce from Table I by comparing the ratios of the total number of trapped charges versus the total number of charges generated in the device  $\nu_{TC}$  for morphology D. To investigate this aspect in more detail, we further consider in Table I the ratio of the total number of charge losses versus the total number of generated charges  $\nu_{TL}$  as well as its different contributions in case of morphologies D and E for different circuit conditions. From the short-circuit results of morphology D, we conclude that significant charge accumulation is hindered in this case by the high percentage of charge losses due to external recombinations  $\nu_{ER}$ , precluding the accumulation of trapped charges in the defects. These ER processes are caused by the annihilation of free charge carriers as a result of the recombination of externally injected charges with internally generated charges produced at the DA heterojunction in the device. This in turn reduces the number of charge losses due to internal recombinations, as can be deduced from the respective ratio of the number of charge losses resulting from internal recombinations versus the to-

TABLE I. Ratio of the number of lost charges through the number of generated charges for the DA-polymer blend PPDI-DTT-biTV-PT in case of the morphologies D and E under open-circuit (oc), short-circuit (sc), as well as real-circuit (rc) conditions, obtained with the DMC-CHC-TDGL method. The total ratio of lost charges  $\nu_{TL}$  is decomposed in contributions from charge losses resulting from internal recombinations  $\nu_{IR}$ , external recombinations  $\nu_{ER}$ , as well as trapped charges  $\nu_{TC}$ .

Morphology	$\nu_{TL}$ (%)	$\nu_{IR}$ (%)	$\nu_{ER}$ (%)	$\nu_{TC}$ (%)
D (sc)	32.2	21.0	9.5	1.7
D (rc)	62.2	47.2	3.1	11.9
D (oc)	56.2	45.0	...	11.2
E (sc)	18.4	16.4	1.7	0.3
E (rc)	23.4	19.6	1.5	2.3
E (oc)	19.6	17.6	...	2.0

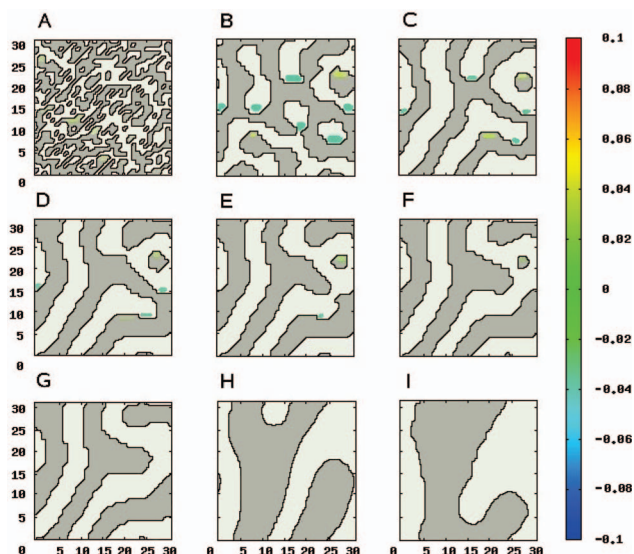


FIG. 5. Charge density of the phase-separated DA-polymer blend PPDI-DTT-biTV-PT for morphologies with different scale of phase separation under short-circuit conditions, obtained either with the DMC-CHC-TDGL (A-H) or the DMC-CHC-SCFT method (I) [light grey: A phase (electron conducting); dark grey: D phase (hole conducting)]. Electrodes are applied in horizontal direction for all morphologies.

tal number of generated charges  $\nu_{IR}$ . Moreover, from the 2D diagram in Fig. 5 of the corresponding charge density for the different morphologies, we conclude that the charge accumulation at the structural defects are reduced under short-circuit conditions, leading to a weakening of the internal electrical fields. This causes a decreased electrostatic attraction of opposite charges and, thus, may also contribute to the improved charge transport efficiency. By comparing these observations to the charge recombination frequency for the same morphologies under real-circuit conditions in Figs. 6(a) and 6(b) we infer that the strong charge accumulation at the defects for morphologies D and E is a consequence of the constant charge-injection rate at the electrodes, restricting the amount of external charge recombinations. The latter finding is confirmed by the lower values for  $\nu_{ER}$ , provided in Table I, in the real-circuit case compared to the short-circuit case. As a result, the process of charge recombination cannot keep pace with the charge-separation process through exciton dissociation at these locations, leading to a strong charge accumulation. This ultimately entails a significant deterioration of the charge transport and drop of the IQE caused by the generation of internal electrical fields. Charges, which have been generated near to a region of high charge density, are more likely to recombine through Coulombic attraction with opposite charges, which have been generated through charge separation in a nearby DA-interface region or injected from the electrodes. Moreover, we see that the exciton dissociation frequency is reduced in the region of high charge density, as can be inferred from Fig. 6(c) for the morphology D. This relates to the fact that charge separation is hindered due to the pressure flow of charges, which aim to travel to the opposite electrode but are trapped in the defect and in this way prevent further charge-separation processes at the DA interface. Both characteristics, i.e., a low

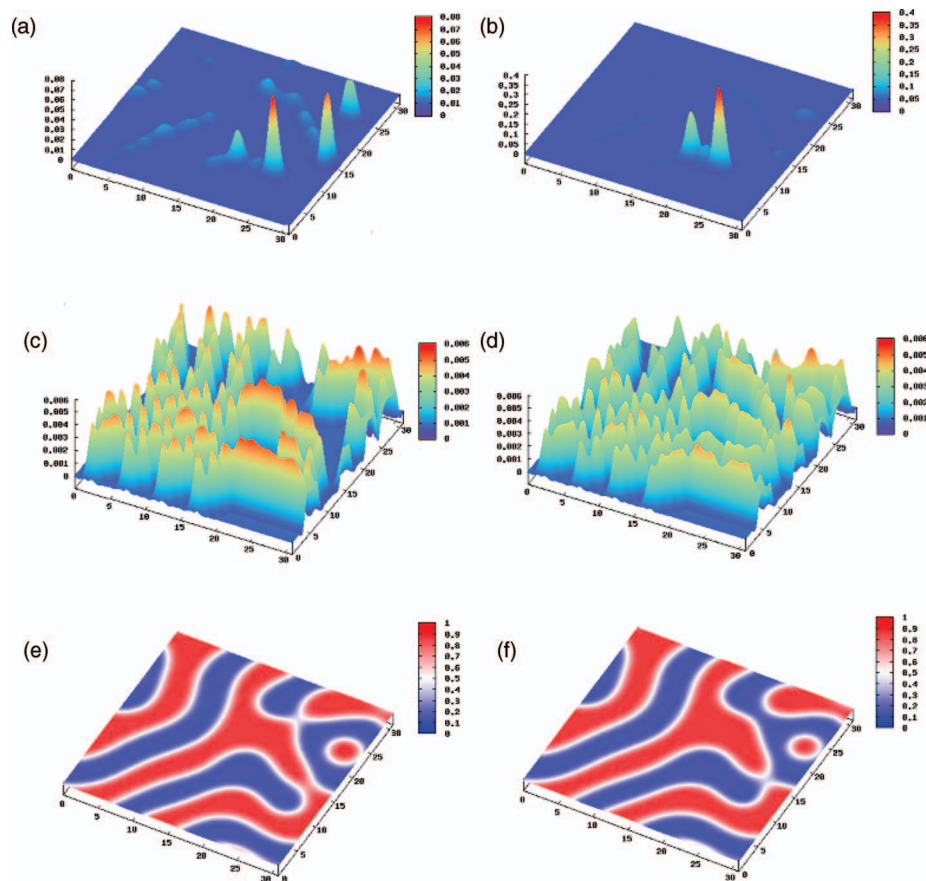


FIG. 6. Frequencies of charge recombination (a,b) and exciton dissociation (c,d) as a function of the volume fractions of the monomer types (e,f), obtained with the DMC-CHC-TDGL method, for the DA-polymer blend PPDI-DTT-biTV-PT in case of the morphologies D (left) and E (right) under real-circuit conditions [red: A phase (electron conducting); blue: D phase (hole conducting)].

exciton dissociation efficiency and a high charge recombination frequency, are a consequence of charge traps in the defects and lead to charge losses, reducing the IQE and power conversion efficiency (PCE) as depicted in Figs. 3(c) and 7, respectively. The nanostructure with the maximum IQE and PCE corresponds to the morphology F, in which all major traps of electrons and holes have disappeared and continuous percolation paths allow a nearly unperturbed flow of the charge carriers to the electrodes. In such an optimal morphology no charges are accumulated or lost due to charge recombinations, as can be concluded from Fig. 4 (morphology F), while an optimal phase thickness for exciton dissociations is guaranteed. The elimination of the nanoscale defect structures from morphologies D to F causes an increase of about 1.23% in the PCE, 24% in the IQE, and 55% in the charge transport efficiency under real-circuit conditions. These observations are in agreement with the experimental findings of Snaith *et al.*,<sup>39</sup> who found through composition analysis and photoluminescence emission spectroscopy experiments on PFB/F8BT-polymer blends that the process of charge transport and not the process of charge generation is the limiting factor of the device performance. We should also point out in this context that several recent experimental and theoretical studies<sup>4,27,37,38,40,42</sup> have demonstrated that structural characteristics can strongly affect the processes of charge generation and recombination as well

as charge transport to the electrodes. Moreover, it is well-established that structural inhomogeneities, such as bottlenecks and dead ends, generally are created during the process of fabrication and can have a significant influence on the photovoltaic efficiency of nanostructured DA-polymer blends.<sup>8,27</sup> To eliminate such inhomogeneities in the experiment, different techniques have been conceived in the past decades, which permit to produce idealized morphologies free of defects. One strategy is to rearrange the nanophases using electrical fields. Russell *et al.*<sup>27,64</sup> could demonstrate in this way that defect-free nanostructures of diblock copolymers can be generated. A further procedure is controlled annealing. By applying this technique to PFB/F8BT blends, McNeill *et al.*<sup>65</sup> observed a dependence of the dynamics of charge generation on the degree of phase separation. They found that the device performance for a phase-separation length of 20 nm is optimal, which is significantly larger than the average exciton diffusion length of 5–10 nm considered in previous works. In further studies it has been speculated that charge transport can also be affected by intra-molecular defects, such as kinks and chemical impurities.<sup>41</sup> Such defects may increasingly be important in confined regions of the morphology with strong variation in composition of the DA-polymer blend, i.e., in bottlenecks and dead ends. Moreover, it is also worth emphasizing that blend systems are generally limited in their usefulness for flexible device applications due to their morphological instability,<sup>33</sup>

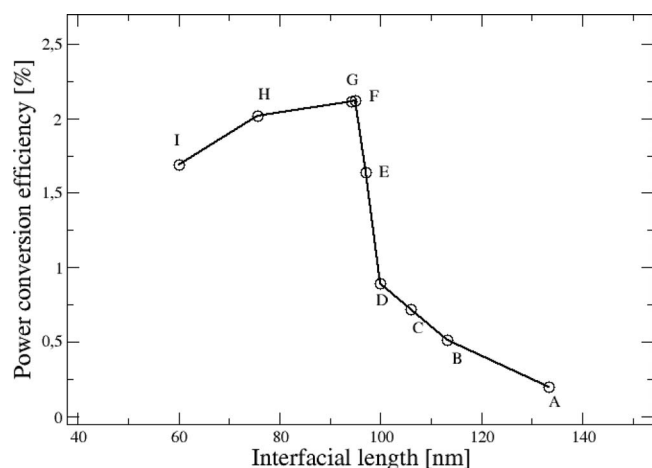


FIG. 7. Power conversion efficiency for the DA-polymer blend PPDI-DTT-biTV-PT as a function of interfacial length under real-circuit conditions, obtained with the DMC-CHC-TDGL method.

conferring poor mechanical properties and thermal stability.<sup>66</sup> They are often kinetically trapped in metastable states and their domains are known to migrate thermally, causing the disruption as well as aggregation of domains on timescales relevant for OPV applications. This may result in the formation of domains of microscopic or even macroscopic size in the D- and A-material. Moreover, their instability and low interpenetrability can reduce the interfacial area between both materials, increasing the diffusion length excitons must travel before charge separation can occur. In ultrathin polymer-blend films the morphological evolution might further be stimulated by surface deformation modes,<sup>67</sup> induced through the release of residual stresses resulting from the fabrication process, non-equilibrium interactions with other device components, an externally applied mechanical strain or electrical fields.

To stabilize the nanostructured BHJ morphology, one possibility is to make use of block copolymers. Below the order-disorder transition temperature, they form a network of physically stable crosslinks by accomplishing a thermodynamic phase-separation process, providing long-time stable morphologies with finer scale and higher performance compared to polymer blends.<sup>68</sup> For example, Sun *et al.*<sup>20</sup> showed that a photovoltaic device composed of a thin film of a donor-bridge-acceptor-bridge-type block copolymer exhibits a significant performance improvement over its corresponding DA blend, i.e., the open-circuit voltage  $V_{oc}$  increased from 0.14 to 1.1 V and the short-circuit current  $J_{sc}$  increased from 0.017 to 0.058 mA cm<sup>-2</sup> under identical conditions. In this system the donor consisted of an alkyl-derivatized poly-*p*-phenylenevinylene (PPV) conjugated block, whereas the acceptor and bridge were composed of a sulfone-alkyl derivatized PPV conjugated block as well as a nonconjugated and flexible unit, respectively. They explained the major improvements in the photovoltaic properties by the block-copolymer intrinsic nanophase-separation process and molecular self-assembly that leads to a reduction of the exciton and charge carrier losses. In another work Lindner *et al.*<sup>18</sup> compared the performance of a block-copolymer device, composed of blocks of the hole-conducting poly(vinyl-triphenyl-amine) and electron-conducting poly(perylene-bisimide-acrylate),

to a device made from a blend with identical composition and phase thickness. They demonstrated that the photovoltaic properties of the block copolymer significantly surpass those of the blend device. More specifically, the device performance parameters  $J_{sc}$  and  $V_{oc}$  were found to improve from 0.028 mA cm<sup>-2</sup> and 0.525 V for the blend to 0.19 mA cm<sup>-2</sup> and 0.865 V for the block copolymer, respectively. Moreover, the PCE was increased by one order of magnitude from 0.007% in the polymer blend to 0.07% in the block-copolymer device. However, it is well known that even with block-copolymer technologies perfect periodic domain ordering is generally achieved only over micron-sized regions, separated by grain boundaries.<sup>67</sup> To provide an estimate for the influence of defects on the length scales of grain boundaries, new simulation approaches will have to be developed, offering guidance to experimentalists and new perspectives for the design of OPV devices with optimized performance.

#### IV. SUMMARY AND OUTLOOK

In summary, in this work we present a new methodology to treat loss processes of charge carriers and excitons in defect structures, affecting the performance of polymer solar cells. Our approach is based on combining either the time-dependent Ginzburg-Landau method or the self-consistent field theory method, to generate morphologies of different scale of phase separation and degree of defect formation, with a dynamical Monte Carlo method, to simulate the elementary photovoltaic processes involving the charge carriers and excitons in a particle description. We apply the new approach on a novel phase-separated nanostructured polymer blend, based on the electron-donating compound bis(thienylenevinylene)-substituted polythiophene and the electron-accepting compound poly(perylene diimide-alt-dithienothiophene). We find that structural inhomogeneities, such as inclusions and dead ends, significantly affect the internal quantum efficiency of the photovoltaic system. These are usually generated in course of the phase-separation process and are inherent artifacts produced during the fabrication procedure. More specifically, we observe that the disjunction of continuous percolation paths leads to the creation of dead ends, which cause severe charge carrier losses through charge recombination lowering the charge transport efficiency in a decisive way. At the same time, we find that dead ends are characterized by a low exciton dissociation efficiency due to a high accumulation of charge carriers, counteracting the charge generation process. From these observations, we conclude that both loss phenomena lead to a dramatic decrease in the internal quantum efficiency. Finally, by analyzing the photovoltaic behavior of the nanostructures under different circuit conditions we demonstrate that charge injection crucially determines the impact of the inhomogeneities on the solar cell performance.

To conclude, we anticipate that the new methodology will permit to predict the photovoltaic efficiency from nanostructured morphologies of complex polymer architectures, providing guidance for the design of new semiconducting polymer compounds with optimized opto-electronic properties. Moreover, in our future work novel multiscale modeling

techniques<sup>69,70</sup> will be developed, to engineer and tune the device performance with regard to the material's behavior.

## ACKNOWLEDGMENTS

The work was supported by the Deutsche Forschungsgemeinschaft (DFG) through Grant No. BA 2256/3-1.

- <sup>1</sup>M. Sommer, S. M. Lindner, and M. Thelakkat, *Adv. Funct. Mater.* **17**, 1493 (2007).
- <sup>2</sup>C. J. Brabec, J. A. Hauch, P. Schilinsky, and C. Waldauf, *MRS Bull.* **30**, 50 (2005).
- <sup>3</sup>C. W. Tang, *Appl. Phys. Lett.* **48**, 183 (1986).
- <sup>4</sup>P. K. Watkins, A. B. Walker, and G. L. B. Verschoor, *Nano Lett.* **5**, 1814 (2005).
- <sup>5</sup>A. C. Mayer, S. R. Scully, B. E. Hardin, M. W. Rowell, and M. D. McGehee, *Mater. Today* **10**, 28 (2007).
- <sup>6</sup>M. Hilczler and M. Tachiya, *J. Phys. Chem. C* **114**, 6808 (2010).
- <sup>7</sup>C.-W. Chu, Y. Shao, V. Shrotriya, and Y. Yang, *Appl. Phys. Lett.* **86**, 243506 (2005).
- <sup>8</sup>P. Peumans, S. Uchida, and S. R. Forrest, *Nature (London)* **425**, 158 (2003).
- <sup>9</sup>S. Uchida, J. Xue, B. P. Rand, and S. R. Forrest, *Appl. Phys. Lett.* **84**, 4218 (2004).
- <sup>10</sup>M. Granstrom, K. Petritsch, A. C. Arias, A. Lux, M. R. Andersson, and R. H. Friend, *Nature (London)* **395**, 257 (1998).
- <sup>11</sup>J. J. M. Halls, C. A. Walsh, N. C. Greenham, E. A. Marseglia, R. H. Friend, S. C. Moratti, and A. B. Holmes, *Nature (London)* **376**, 498 (1995).
- <sup>12</sup>T. Kietzke, H.-H. Hörhold, and D. Neher, *Chem. Mater.* **17**, 6532 (2005).
- <sup>13</sup>A. J. Breeze, A. Salomon, D. S. Ginley, B. A. Gregg, H. Tillmann, and H.-H. Hörhold, *Appl. Phys. Lett.* **81**, 3085 (2002).
- <sup>14</sup>G. Yu, J. Gao, and J. C. Hummelen, *Science* **270**, 1789 (1995).
- <sup>15</sup>J.-I. Nakamura, C. Yokoe, K. Murata, and K. Takahashi, *J. Appl. Phys.* **96**, 6878 (2004).
- <sup>16</sup>C. J. Brabec, N. S. Sariciftci, and J. C. Hummelen, *Adv. Funct. Mater.* **11**, 15 (2001).
- <sup>17</sup>W. Ma, C. Yang, X. Gong, K. Lee, and A. J. Heeger, *Adv. Funct. Mater.* **15**, 1617 (2005).
- <sup>18</sup>S. M. Lindner, S. Hüttner, A. Chiche, M. Thelakkat, and G. Krausch, *Angew. Chem. Int. Ed.* **45**, 3364 (2006).
- <sup>19</sup>Y. Sun, S.-C. Chien, H.-L. Yip, K.-S. Chen, Y. Zhang, J. A. Davies, F.-C. Chen, B. Lin, and A. K.-Y. Jen, *J. Mater. Chem.* **22**, 5587 (2012).
- <sup>20</sup>S.-S. Sun, C. Zhang, A. Ledbetter, S. Choi, K. Seo, and J. Haliburton, *Appl. Phys. Lett.* **90**, 043117 (2007).
- <sup>21</sup>S. Sun, Z. Fan, Y. Wang, and J. Haliburton, *J. Mater. Sci.* **40**, 1429 (2005).
- <sup>22</sup>S.-S. Sun, Z. Fan, Y. Wang, K. Winston, and C. E. Bonner, *Mater. Sci. Eng. B* **116**, 279 (2005).
- <sup>23</sup>M. D. McGehee and M. A. Topinka, *Nature Mater.* **5**, 675 (2006).
- <sup>24</sup>H. Hoppe and N. S. Sariciftci, *J. Mater. Chem.* **16**, 45 (2006).
- <sup>25</sup>K. Sivula, Z. T. Ball, N. Watanabe, and J. M. J. Frechet, *Adv. Mater.* **18**, 206 (2006).
- <sup>26</sup>M. Drees, H. Hoppe, C. Winder, H. Neugebauer, N. S. Sariciftci, W. Schwinger, F. Schäffler, C. Topf, M. C. Scharber, Z. Zhu, and R. Gaudiana, *J. Mater. Chem.* **15**, 5158 (2005).
- <sup>27</sup>G. A. Buxton and N. Clarke, *Phys. Rev. B* **74**, 085207 (2006).
- <sup>28</sup>U. Scherf, A. Gutacker, and N. Koenen, *Acc. Chem. Res.* **41**, 1086 (2008).
- <sup>29</sup>R. A. Segalman, B. McCulloch, S. Kirmayer, and J. J. Urban, *Macromolecules* **42**, 9205 (2009).
- <sup>30</sup>S. B. Darling, *Energy Environ. Sci.* **2**, 1266 (2009).
- <sup>31</sup>M. Sommer, S. Huettner, and M. Thelakkat, *J. Mater. Chem.* **20**, 10788 (2010).
- <sup>32</sup>I. Botiz and S. B. Darling, *Mater. Today* **13**, 42 (2010).
- <sup>33</sup>P. D. Topham, A. J. Parnell, and R. C. Hiorns, *J. Polym. Sci. Part B: Polym. Phys.* **49**, 1131 (2011).
- <sup>34</sup>S. M. Lindner and M. Thelakkat, *Macromolecules* **37**, 8832 (2004).
- <sup>35</sup>G. Tu, H. Li, M. Forster, R. Heiderhoff, L. J. Balk, and U. Scherf, *Macromolecules* **39**, 4327 (2006).
- <sup>36</sup>M. H. van der Veen, B. de Boer, U. Stalmach, K. I. van de Wetering, and G. Hadziioannou, *Macromolecules* **37**, 3673 (2004).
- <sup>37</sup>D. C. Coffey and D. S. Ginger, *Nature Mater.* **5**, 735 (2006).
- <sup>38</sup>D. Coffey and D. S. Ginger, SPIE Newsroom, 27 February 2007.
- <sup>39</sup>H. J. Snaith, A. C. Arias, A. C. Morteani, C. Silva, and R. H. Friend, *Nano Lett.* **2**, 1353 (2002).
- <sup>40</sup>C. R. McNeill, B. Watts, L. Thomsen, W. J. Belcher, N. C. Greenham, and P. C. Dastoor, *Nano Lett.* **6**, 1202 (2006).
- <sup>41</sup>D. Wang, M. Reese, N. Kopidakis, and B. A. Gregg, NREL/CP-270-42565, May 2008.
- <sup>42</sup>G. A. Buxton and N. Clarke, *Model. Simul. Mater. Sci. Eng.* **15**, 13 (2007).
- <sup>43</sup>B. A. Gregg and M. C. Hanna, *J. Appl. Phys.* **93**, 3605 (2003).
- <sup>44</sup>J. A. Barker, C. M. Ramsdale, and N. C. Greenham, *Phys. Rev. B* **67**, 075205 (2003).
- <sup>45</sup>J. O. Haerter, S. V. Chasteen, S. A. Carter, and J. C. Scott, *Appl. Phys. Lett.* **86**, 164101 (2005).
- <sup>46</sup>R. A. Marsh, C. Groves, and N. C. Greenham, *J. Appl. Phys.* **101**, 083509 (2007).
- <sup>47</sup>R. K. Cavin, V. V. Zhirnov, G. I. Bourianoff, J. A. Hutchby, D. J. C. Herr, H. H. Hosack, W. H. Joyner, and T. A. Wooldridge, *J. Nanopart. Res.* **7**, 573 (2005).
- <sup>48</sup>S. A. Baeurle, G. H. Fredrickson, and A. A. Gusev, *Macromolecules* **37**, 5784 (2004).
- <sup>49</sup>L. Delle Site, C. F. Abrams, A. Alavi, and K. Kremer, *Phys. Rev. Lett.* **89**, 156103 (2002).
- <sup>50</sup>L. Delle Site, S. Leon, and K. Kremer, *J. Am. Chem. Soc.* **126**, 2944 (2004).
- <sup>51</sup>J. Kirkpatrick, V. Marcon, J. Nelson, K. Kremer, and D. Andrienko, *Phys. Rev. Lett.* **98**, 227402 (2007).
- <sup>52</sup>S. C. Glotzer and W. Paul, *Annu. Rev. Mater. Res.* **32**, 401 (2002).
- <sup>53</sup>H. Tang and K. F. Freed, *J. Chem. Phys.* **94**, 6307 (1991).
- <sup>54</sup>M. Doi, *Macromol. Symposia* **195**, 101 (2003).
- <sup>55</sup>F. Schmid, "Theory and simulation of multiphase polymer systems," in *Handbook of Multiphase Polymer Systems*, edited by A. Boudenne, L. Ibos, Y. Candau, and S. Thomas (Wiley, Chichester, 2011), Chap. 3.
- <sup>56</sup>T. Kawakatsu, *OCTA Integrated Simulation System for Soft Materials*, User's Manual, Version 8.0, 2009, Chap. 7, p. 134.
- <sup>57</sup>See <http://octa.jp/> for information about OCTA-program.
- <sup>58</sup>D. T. Gillespie, *Annu. Rev. Phys. Chem.* **58**, 35 (2007).
- <sup>59</sup>L. Meng, Y. Shang, Q. Li, Y. Li, X. Zhan, Z. Shuai, R. G. E. Kimber, and A. B. Walker, *J. Phys. Chem. B* **114**, 36 (2010).
- <sup>60</sup>X. Zhan, Z. Tan, B. Domercq, Z. An, X. Zhang, S. Barlow, Y. Li, D. Zhu, B. Kippelen, and S. R. J. Marder, *J. Am. Chem. Soc.* **129**, 7246 (2007).
- <sup>61</sup>R. A. Marcus, *Rev. Mod. Phys.* **65**, 599 (1993).
- <sup>62</sup>K. Seki and M. Tachiya, *Phys. Rev. B* **65**, 014305 (2001).
- <sup>63</sup>R. G. E. Kimber, A. B. Walker, G. E. Schröder-Turk, and D. J. Cleaver, *Phys. Chem. Chem. Phys.* **12**, 844 (2010).
- <sup>64</sup>T. L. Morkved, M. Lu, A. M. Urbas, E. E. Ehrichs, H. M. Jaeger, P. Mansky, and T. P. Russell, *Science* **273**, 931 (1996).
- <sup>65</sup>C. R. McNeill, S. Westenhoff, C. Groves, R. H. Friend, and N. C. Greenham, *J. Phys. Chem. C* **111**, 19153 (2007).
- <sup>66</sup>D. Pospiech, "Influencing the interface in polymer blends by compatibilization with block copolymers," in *Polymer Surfaces and Interfaces*, edited by M. Stamm (Springer, Berlin, 2008), pp. 275–298.
- <sup>67</sup>R. Mukherjee, A. Sharma, and U. Steiner, "Surface instability and pattern formation in thin polymer films," in *Generating Micro- and Nanopatterns on Polymeric Materials*, edited by A. del Campo and A. Arzt (Wiley-VCH, Weinheim, 2011), p. 246.
- <sup>68</sup>J. Peet, M. L. Senatore, A. J. Heeger, and G. C. Bazan, *Adv. Mater.* **21**, 1521 (2009).
- <sup>69</sup>S. A. Baeurle, *J. Math. Chem.* **46**, 363 (2009).
- <sup>70</sup>S. A. Baeurle, T. Usami, and A. A. Gusev, *Polymer* **47**, 8604 (2006).